Analytical description of tidal dynamics in convergent estuaries

4 authors, including:

Hubert H. G. Savenije
Delft University of Technology
462 PUBLICATIONS   **23,282** CITATIONS

SEE PROFILE

Marco Toffolon
Università degli Studi di Trento
112 PUBLICATIONS   **2,195** CITATIONS

SEE PROFILE

E. J. M. Veling
Delft University of Technology
60 PUBLICATIONS   **952** CITATIONS

SEE PROFILE

Some of the authors of this publication are also working on these related projects:

Project   Vertical DTS profiles of air temperature, wind speed, and wet bulb temperature View project

Project   Science for Management of Ypacaraí Lake's Eutrophication (SMYLE) View project

Analytical description of tidal dynamics in convergent estuaries

Hubert H. G. Savenije,[1,2] Marco Toffolon,[3] Jennifer Haas,[1] and Ed J. M. Veling[1]

[1] Analytical solutions of the one-dimensional hydrodynamic equations for tidal wave propagation are now available and, in this paper, presented in explicit equations. For given topography, friction, and tidal amplitude at the downstream boundary, the velocity amplitude, the wave celerity, the tidal damping, and the phase lag can be computed. The solution is based on the full nonlinearized St. Venant equations applied to an exponentially converging channel, which may have a bottom slope. Two families of solutions exist. The first family consists of mixed tidal waves, which have a phase lag between zero and $\pi/2$, which occur in alluvial coastal plain estuaries with almost no bottom slope; the second family consists of "apparent standing" waves, which develop in short estuaries with a steep topography. Asymptotic solutions are presented for progressive waves, frictionless waves, waves in channels with constant cross section, and waves in ideal estuaries where there is no damping or amplification. The analytical method is accurate in the downstream, marine part of estuaries and particularly useful in combination with ecological or salt intrusion models. The solutions are compared with observations in the Schelde, Elbe, and Mekong estuaries.

1. Introduction

[2] Ever since Barré de Saint-Venant published his equations for viscous flow in 1843, efforts have been made to solve the set of equations analytically. At first, out of need. Analytical solutions were the only option to turn the nonlinear partial differential equations into practical applications. In river systems, the equations could in general be simplified more easily than in tidal water bodies. Rivers tend to have more or less constant cross sections and in large rivers temporal gradients are slow. As a result, quasi steady state solutions or strongly linearized solutions appeared to work rather well in rivers, leading to analytical expressions for backwater curves, and the kinematic wave solution. In tidal water bodies, however, quasi steady state could not be assumed.

[3] A fruitful attempt was made by Lorentz, the 1902 Nobel prize winner for physics, who linearized the equations, introducing his linearized friction factor, and solved them in 1919 to compute the effects of a closure dam on the Dutch Zuyderzee, now Ijssel lake. *Ippen* [1966] and *Harleman* [1966] solved the St. Venant equations for estuaries with constant cross section and estuaries with an exponentially varying cross sections (which they called "real estuaries"),

respectively. However, they used the linearized equations, with linearized friction and a horizontal bottom. As a result their solutions were not very accurate.

[4] With the appearance on the scene of the digital computer, in the 1970s, the need for analytical solutions subsided. The quest for analytical solutions continued, but at a slower pace. The trigger seemed to be curiosity rather than necessity. Still, there were a number of good reasons for finding analytical solutions. First there is the insight that analytical equations provide. It is possible to see directly what the impact of an intervention, such as dredging, is on the tidal dynamics and one can see how a certain parameter affects another. Analytical equations are not only good for educational purposes, but also to assess the outcome of numerical models or to design a model setup or field research.

[5] The analytical solutions developed to date, concerning one-dimensional models, all require a certain number of assumptions on topography and flow characteristics. In tidal hydraulics, the cross section is usually assumed as constant (rectangular, trapezoidal, or triangular) or gradually varying, with an exponential (or power law) longitudinal variation. Moreover, the tidal range to depth ratio is assumed much less than unity, the Froude number small, and the freshwater discharge small compared to tidal flows. Such common assumptions are shared also by recent approaches, such as by *Jay* [1991], *Friedrichs and Aubrey* [1994], *Lanzoni and Seminara* [1998], *Prandle* [2003], and *Savenije* [2005]. The difference is that most authors use perturbation analysis, where the scaled equations are simplified by neglecting higher-order terms, whereas *Savenije* [2005] uses a simple harmonic solution without simplifying the equations. Both

---

[1]Department of Water Management, Delft University of Technology, Delft, Netherlands.
[2]UNESCO-IHE Institute for Water Education, Delft, Netherlands.
[3]Department of Civil and Environmental Engineering, University of Trento, Trento, Italy.
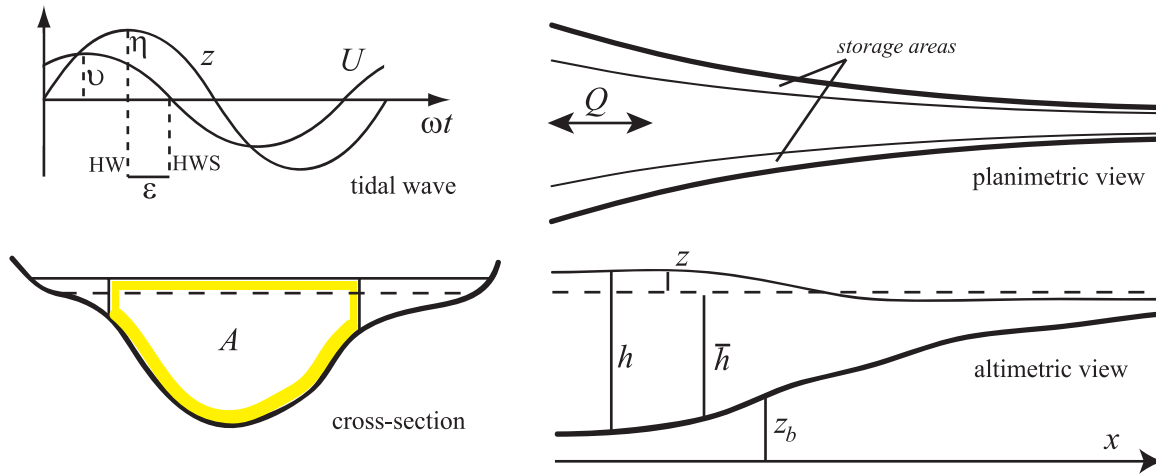
Figure 1. Sketch and notation.

methods give good results as long as the tidal range to depth ratio is small.

[6] In this paper we use an exponentially varying cross section, allowing for bottom slope, in combination with the complete nonlinearized St. Venant equations. The methodology makes use of the set of implicit analytical equations presented by *Savenije* [2005] which is solved explicitly and compared to observed tidal parameters in three different estuaries: the Schelde in The Netherlands, the Elbe in Germany, and the Tien and Hau (the two main branches of the Mekong) in Vietnam. The relatively simple explicit equations obtained are potentially powerful in combination with ecological or salt intrusion models, or to obtain first-order estimates of the consequences of interventions in estuary topography (e.g., by dredging).

2. Formulation of the Problem

[7] The conceptual sketch of the one-dimensional model of tidal wave propagation presented in this contribution is shown in Figure 1, where x is the longitudinal coordinate measured in landward direction from the mouth of the estuary, h is the flow depth, z is the water level fluctuation, z_b is bottom elevation, A is the cross-sectional area of the stream profile. The ratio between the storage width and the stream width is r_S. Hereinafter, an over-bar denotes tidally averaged variables: thus $\overline{h}$ is the tidal average depth of flow and $\overline{A}$ is the tidal average cross-sectional area. Moreover, we define Q as the tidal flow discharge, U as the tidal flow velocity, ρ as the water density.

[8] In the following, we consider a sinusoidal tidal wave having a tidal period T, a frequency $\omega = 2\pi/T$, and a wavelength $L = cT$, being c the wave celerity. As schematically shown in Figure 1, υ is the amplitude of the tidal velocity U, and η is the amplitude of the tidal water level variation z. Another important parameter describing the tidal wave is the phase lag ε between high water (HW) and high water slack (HWS) (or between low water (LW) and low water slack (LWS)). For a simple harmonic wave, $\varepsilon = \pi/2 - (\phi_z - \phi_U)$, where ϕ_z is the phase of water level and ϕ_U the phase of velocity.

2.1. Basic Equations

[9] The tidal dynamics in an alluvial estuary can be described by the following set of one-dimensional equations [e.g., *Savenije*, 2005]:

$$\frac{\partial U}{\partial t} + U\frac{\partial U}{\partial x} + g\frac{\partial h}{\partial x} + g\frac{\partial z_b}{\partial x} - g\frac{h}{2\rho}\frac{\partial \rho}{\partial x} + g\frac{U|U|}{C^2 h} = 0, \quad (1)$$

$$r_S\frac{\partial A}{\partial t} + \frac{\partial Q}{\partial x} = 0, \quad (2)$$

where g is the acceleration due to gravity, C is Chezy's friction factor; the longitudinal gradient of the water density ρ drives a residual water surface slope. In the derivation of these equations two assumptions have been used, the first being that the Froude number is O(0.1) or smaller. Subsequently a second necessary assumption is that the channel is well-defined and that $r_S < 2$. If not, then the second term in equation (1) needs to be modified.

[10] For the purpose of scaling, we rewrite equations (1) and (2) considering z as the water level fluctuation in relation to the tidal average water level:

$$h = z + \overline{h}. \quad (3)$$

Assuming that the depth convergence is small compared to the width convergence and the tidal amplitude to depth ratio is small, equations (1) and (2) can be modified into

$$\frac{\partial U}{\partial t} + U\frac{\partial U}{\partial x} + g\frac{\partial z}{\partial x} + g\sigma + g\frac{U|U|}{C^2 h} = 0, \quad (4)$$

$$rs\frac{\partial z}{\partial t} + U\frac{\partial z}{\partial x} + h\frac{\partial U}{\partial x} + \frac{hU}{\overline{A}}\frac{\partial \overline{A}}{\partial x} = 0, \quad (5)$$

where $\sigma = \partial(z_b + \overline{h})/\partial x - h/(2\rho)\partial\rho/\partial x$ includes the free surface residual slope and the density term.

[11] In alluvial estuaries, the tidal average cross-sectional area $\overline{A}$ can be well described by an exponential function

$$\overline{A} = \overline{A}_0 \exp\left(-\frac{x}{a}\right), \tag{6}$$

where $\overline{A}_0$ is the cross-sectional area at the origin (the mouth of the estuary) and a is the convergence length. Equation (5) then modifies into

$$r_S \frac{\partial z}{\partial t} + U \frac{\partial z}{\partial x} + h \frac{\partial U}{\partial x} - \frac{hU}{a} = 0. \tag{7}$$

2.2. Scaling the Equations

[12] In this section we aim at identifying the dimensionless parameters that can be used to describe the tidal wave characteristics in a given reach of the estuary, where suitable reference values of the main quantities are adopted as constant scales. Thus we introduce a scaling on equations (4) and (7), similar to that used by *Toffolon et al.* [2006], to derive dimensionless equations, the asterisk superscript denoting dimensionless variables:

$$U = \upsilon U^*, \quad h = \overline{h}h^*, \quad z = \eta z^*, \quad x = \frac{L}{2\pi}x^*, \quad t = \frac{T}{2\pi}t^*,$$

$$C = \sqrt{\frac{g}{f}}C^*, \quad \sigma = \frac{\overline{h}}{L}\sigma^*, \tag{8}$$

where the scales have been already introduced and f is the dimensionless friction factor. The residual slope and density term σ, although already dimensionless, is rescaled with the depth to length ratio. Assuming that the adopted scales are constant in the domain of solution, we obtain

$$\frac{\partial U^*}{\partial t^*} + \left(\frac{\upsilon T}{L}\right)U^* \frac{\partial U^*}{\partial x^*} + \left(\frac{g\eta T}{\upsilon L}\right)\frac{\partial z^*}{\partial x^*} + \left(\frac{gT\overline{h}}{\upsilon L}\right)\sigma^*$$

$$+ \left(\frac{\upsilon Tf}{2\pi\overline{h}}\right)\frac{U^*|U^*|}{C^{*2}h^*} = 0, \tag{9}$$

$$\frac{\partial z^*}{\partial t^*} + \left(\frac{\upsilon T}{Lr_S}\right)U^* \frac{\partial z^*}{\partial x^*} + \left(\frac{\overline{h}\upsilon T}{\eta Lr_S}\right)h^* \frac{\partial U^*}{\partial x^*} - \left(\frac{\overline{h}\upsilon T}{2\pi\eta ar_S}\right)h^*U^* = 0. \tag{10}$$

There is the problem to determine the real scales of velocity (υ) and wavelength (L), so we use the values for a frictionless tidal wave in a channel with zero convergence (U_0, L_0) as a reference:

$$\upsilon = U_0\mu, \tag{11}$$

$$L = L_0/\lambda, \tag{12}$$

where we introduce the unknown velocity number μ and celerity number λ. Moreover, the dimensionless tidal amplitude ζ is defined as

$$\zeta = \eta/\overline{h}. \tag{13}$$

Taking into account the storage effect, the following relationships are valid for the classical wave celerity c_0 (zero convergence and no friction), the frictionless velocity amplitude U_0 and the frictionless wavelength for zero convergence L_0:

$$c_0 = \sqrt{\frac{g\overline{h}}{r_s}}, \tag{14}$$

$$U_0 = \zeta c_0 r_s, \tag{15}$$

$$L_0 = c_0 T. \tag{16}$$

Thus the dimensionless equations read

$$\frac{\partial U^*}{\partial t^*} + r_S \zeta\mu\lambda U^* \frac{\partial U^*}{\partial x^*} + \frac{\lambda}{\mu}\frac{\partial z^*}{\partial x^*} + \frac{\lambda}{\zeta\mu}\sigma^* + \mu\chi\frac{U^*|U^*|}{C^{*2}h^*} = 0, \tag{17}$$

$$\frac{\partial z^*}{\partial t^*} + \zeta\mu\lambda U^* \frac{\partial z^*}{\partial x^*} + \mu\lambda h^* \frac{\partial U^*}{\partial x^*} - \mu\gamma h^*U^* = 0, \tag{18}$$

where the dimensionless parameters χ and γ have been introduced as the friction number and estuary shape number, respectively:

$$\chi = r_S f \frac{c_0}{\omega\overline{h}}\zeta = r_S f \frac{L_0}{2\pi\overline{h}}\zeta, \tag{19}$$

$$\gamma = \frac{c_0}{\omega a} = \frac{L_0}{2\pi a}. \tag{20}$$

The estuary shape number γ depends on the ratio of the square root of the depth to the convergence length and is the main indicator for estuary shape.

[13] Note that equations (14), (15), and (19) are slightly different from the definitions used by *Toffolon et al.* [2006] because they include the effect of the parameter r_s. As a consequence, the corresponding definitions of the velocity number and the celerity number are

$$\mu = \frac{1}{r_S}\frac{\upsilon}{\zeta c_0} = \frac{1}{r_S}\frac{\upsilon\overline{h}}{\eta c_0}, \tag{21}$$

$$\lambda = \frac{L_0}{L} = \frac{c_0}{c}, \tag{22}$$

where $c = L/T$ is the actual celerity of propagation of the tidal wave. Moreover, the definition of γ used by *Toffolon et al.* [2006] only referred to the width convergence, assuming a horizontal bottom, an unnecessary assumption here.

[14] It is interesting to note that the dimensionless form of the governing equations (17) and (18) does not contain r_S explicitly, apart from the second term of equation (17) which is a small term compared to the first term (as long as the Froude number $r_S\zeta\mu$ is small) and hence the effect of

Table 1. Assumptions Made for the Derivation of the Basic Equations

Equation Name	Equation Number	Reference	Assumptions Made[a]
Phase lag equation	(23)	*Savenije* [1992, 1993]	1, 2, 3, 4, 5, 6, 7, 8
Scaling equation	(24)	*Savenije* [1993]	1, 2, 3, 4, 5, 6, 7, 8
Damping equation	(25)	*Savenije* [2001]	1, 2, 3, 4, 5, 6, 7, 8
Celerity equation	(26)	*Savenije and Veling* [2005]	1, 2, 3, 4, 5, 6, 7, 8, 9

[a]Assumptions are as follows, where 1–3 are the basic assumptions: 1, exponentially varying cross section, where a is constant; 2, the tidal amplitude to depth ratio is small ($\zeta < 1$); 3, freshwater discharge is small compared to the tidal flow; 4, small Froude number (this follows directly from assumption 2); 5, simple harmonic function to describe the tide; 6, depth to width ratio is small, and storage width is close to unity ($h/B \ll 1$, $r_S < 2$); 7, the salt intrusion is well-mixed (this is essentially the same as assumption 3); 8, tidal damping is small, that is, $\frac{E}{\eta}\left|\frac{d\eta}{dx}\right| \ll 1$; 9, the phase lag ε and the wave celerity c are constant along an estuary reach (this is the case in an ideal estuary, where damping is small; it is a strict interpretation of assumption 8).

r_S, which is close to unity, may generally be disregarded in this term. If the factor r_S is disregarded in this term, then these equations are identical to the equations used by *Toffolon et al.* [2006], apart from the residual slope and density term.

2.3. Analytical Solutions

[15] Equations (1) and (2) can be written in the form of four implicit analytical equations, as described by *Savenije* [2005, chap. 3]. These derivations are based on earlier papers by *Savenije* [1992, 1993, 1998, 2001] and *Savenije and Veling* [2005]. Table 1 lists the assumptions made in the derivations of these equations. The basic assumption is that the cross-sectional area of the estuary can be described by an exponential function, following equation (6), as is the case in alluvial estuaries (assumption 1). A second fundamental assumption for all equations is that the ratio of the tidal amplitude to depth is less than unity (assumption 2). The third assumption is that the freshwater discharge is small compared to the amplitude of the tidal discharge (assumption 3). Although during a flood situation or in the most upstream part of an estuary this may not always be the case, in exponentially shaped estuaries this is not a restrictive assumption. *Horrevoets et al.* [2004] looked into the validity of this assumption, and concluded that it was acceptable in the downstream, tide dominated, part of alluvial estuaries. The three basic assumptions (assumptions 1, 2, and 3) are quite acceptable for small-amplitude tidal waves in the downstream end of alluvial estuaries. The other assumptions listed in Table 1 are derivatives of these three basic assumptions. The requirement that the Froude number is small (assumption 4) is essentially the same as assumption 2, but less restrictive; the Froude number is generally smaller than the amplitude to depth ratio (see equation (24)). Assumption 5, stating that the tidal wave can be described by a simple harmonic function, follows from assumptions 2 and 3. If the tidal amplitude to depth ratio and the freshwater to tidal discharge ratio are small, then the tidal wave is not much deformed by nonlinear effects, but it is unavoidable that as the wave travels further inland, the wave deforms, resulting in a longer ebb and shorter flood duration. A nonrestrictive assumption is that the width to depth ratio should be large and that the storage width ratio should be modest (assumption 6). This assumption is not really important since it only affects the second term of equation (1) which scales at the Froude number, and moreover alluvial estuaries have a large width to depth ratio. The requirement that the salt intrusion is partially or well mixed (assumption 7) relates to assumption 3, while it

is not a restrictive assumption. Assumption 8 requires that tidal damping is modest. It implies that the length scale of the damping/amplification process is much longer than the distance traveled by a water particle (the tidal excursion E). This assumption is also not restrictive in alluvial estuaries, as is shown empirically [e.g., *Savenije*, 2005]. Some methods require the absence of bottom slope, but this is not a necessary condition in this approach, as long as the bottom slope effect is incorporated in the gradient of the cross-sectional area (i.e., in the convergence length a). Finally, the derivation of the celerity equation through the methods of characteristics [*Savenije and Veling*, 2005] uses the assumptions that the wave celerity and the phase lag between HW and HWS are constant over an estuary reach (assumption 9) and that the tidal wave travels as a simple harmonic function. The latter corresponds with assumption 5, the former is an additional assumption. This assumption corresponds with an ideal estuary where there is no tidal damping or amplification and holds true if assumption 8 is strictly adhered to. Finally, we note that previous authors have proposed relationships which may look similar to the ones summarized in this paper. However, in most cases they are valid only in some limiting cases (see for instance the comments below about *Friedrichs and Aubrey*'s [1994] relationships). The four implicit analytical equations are summarized as follows:

2.3.1. Phase Lag Equation

[16] The phase lag equation is

$$\tan \varepsilon = \frac{\omega a}{c} \left/ \left(1 - \frac{a}{\eta}\frac{d\eta}{dx}\right)\right. , \qquad (23)$$

where c is the celerity of the tidal wave for average depth, not compensating for HW or LW. The phase lag ε is a crucial parameter defining the type of wave occurring in an estuary. If $\varepsilon = 0$, the tidal wave mimics a standing wave; if $\varepsilon = \pi/2$, the tidal wave is a progressive wave. In convergent estuaries the value of ε is always between 0 and $\pi/2$. A wave with a phase lag between 0 and $\pi/2$ is called a "mixed tidal wave" [*Savenije*, 2005]. We can see in equation (23) that if there is modest tidal damping or amplification, the phase lag depends solely on the ratio of the convergence length to the wavelength of the tidal wave ($L = cT$). This equation was derived by *Savenije* [1992, 1993] from the conservation of mass equation (2), using a simple harmonic wave in a Lagrangean reference frame. A similar equation was derived by *Prandle* [2003] for strongly convergent estuaries with a triangular cross section. We also

note that, in the limit of standing waves ($\varepsilon \to 0$) and vanishing amplification, equation (23) becomes $\varepsilon = a\omega/c$, which corresponds to equation (37) of *Friedrichs and Aubrey* [1994].

2.3.2. Scaling Equation

[17] The scaling equation is

$$r_S \frac{\eta}{\bar{h}} = \frac{v}{c} \frac{1}{\sin \varepsilon}, \qquad (24)$$

which introduces the amplitude of the tidal flow velocity, v. This equation, first published by *Savenije and Veling* [2005], makes use of the analytical solution of the conservation of mass equation published by *Savenije* [1993] and equation (23). For a progressive wave, where $\varepsilon = \pi/2$, this equation corresponds with the equation used by other authors [e.g., *Friedrichs and Aubrey*, 1994; *Jay*, 1991] to scale the St. Venant equations. Also for a stranding wave ($\varepsilon \to 0$) with modest amplification, using the simplified version of equation (23) discussed above, equation (24) becomes $v = g\omega\eta a/c_0^2$, which corresponds to equation (11) of *Friedrichs and Aubrey* [1994].

2.3.3. Damping/Amplification Equation

[18] The damping/amplification equation is

$$\frac{1}{\eta} \frac{d\eta}{dx} \left(\frac{1 + \alpha}{\alpha} \right) = \frac{1}{a} - f \frac{v \sin \varepsilon}{\bar{h} c}, \qquad (25)$$

where $\alpha = cv\sin\varepsilon/(g\eta)$ is a tidal Froude number and f is the friction factor defined in equation (8). This equation follows from a combination of equations (1), (2), and (6), and was derived by *Savenije* [2001]. This equation followed from subtraction of the two asymptotic solutions for high water (HW) and low water (LW). The two terms on the right-hand side represent the balance between convergence and friction. If the estuary is strongly convergent and smooth, the tidal wave is amplified; if it is moderately convergent and rough, the tidal wave is damped. In an "ideal" estuary these terms cancel out and there is no tidal damping. In the latter case, the energy gained per unit volume of water by the convergence of the banks is equal to the energy dissipated by friction. In the derivation of this equation the upstream boundary condition used is that channel is infinitely long (no weir or obstruction) and that the freshwater discharge is negligible. *Horrevoets et al.* [2004] solved the equation for a non-negligible discharge, which yielded additional terms in the friction term [see *Savenije*, 2005, section 3.3.3].

2.3.4. Celerity Equation

[19] The celerity equation is

$$c^2 = \frac{1}{r_S} g\bar{h} \Big/ \left[1 - \frac{\sin \varepsilon \cos \varepsilon}{(1 + \alpha)} \left(\frac{c}{\omega a} - f \frac{v \sin \varepsilon}{\omega \bar{h}} \right) \right] = \frac{c_0^2}{1 - D}, \quad (26)$$

where D is the damping term. If the damping term equals zero, then we have an "ideal" estuary where the wave celerity equals the classical wave celerity. As already recognized by previous authors [e.g., *Friedrichs and Aubrey*, 1994], if the damping term is negative, then the

wave is damped and the wave celerity is less than the classical wave celerity; if the damping term is positive, then the wave is amplified and the wave celerity exceeds the classical wave celerity. The upper boundary of the damping term is $D = 1$. This situation corresponds with an "apparently standing wave." This is not the same as a standing wave due to full reflection. In fact, as in the case of a strongly convergent estuary, the incident wave alone results in an infinite wave celerity and, in so doing, mimics a standing wave [*Jay*, 1991].

[20] The celerity equation was derived by *Savenije and Veling* [2005] using the method of characteristics for an amplified or damped tidal wave. Rearranging equations (25) and (26) with equations (23) and (24), after some algebraic manipulations one can find $(c/c_0)^2 - 1 = d\eta/dx(1 - a/\eta \ d\eta/dx)(c/\omega)^2/(a\eta)$; in the case of small amplification, this corresponds to a manipulation of equation (29) by *Friedrichs and Aubrey* [1994].

[21] Hence, a combination of methods was uses to derive the analytical equations. The phase lag equation and the scaling equation are based on a Lagrangean approach, where the integration is made following a water particle. The damping equation followed from substitution of these equations in the momentum balance equation and solving for asymptotic solutions. The fourth equation, however, was derived by the method of characteristics. In combining these approaches inconsistencies may arise, which may limit the applicability of the method. However, since any analytical (linear) solution of the nonlinear equations is an approximation with limited applicability, this may not be a problem, as long as the result is as accurate, or more accurate than the methods used thus far.

2.4. The Governing Dimensionless Equations

[22] These four equations can be scaled making use of the dimensionless parameters derived in section 2.2: the estuary shape number γ given by equation (20), the velocity number μ given by equation (21), the celerity number λ given by equation (22), the friction number χ given by equation (19), and a damping number δ, defined as

$$\delta = \frac{1}{\eta} \frac{d\eta}{dx} \frac{c_0}{\omega}. \qquad (27)$$

Substitution of these dimensionless parameters in equations (23)–(26) yields the following four dimensionless equations:

Phase lag equation

$$\tan \varepsilon = \frac{\lambda}{\gamma - \delta}, \qquad (28)$$

Scaling equation

$$\mu = \frac{\sin \varepsilon}{\lambda} = \frac{\cos \varepsilon}{\gamma - \delta}, \qquad (29)$$

Damping/amplification equation

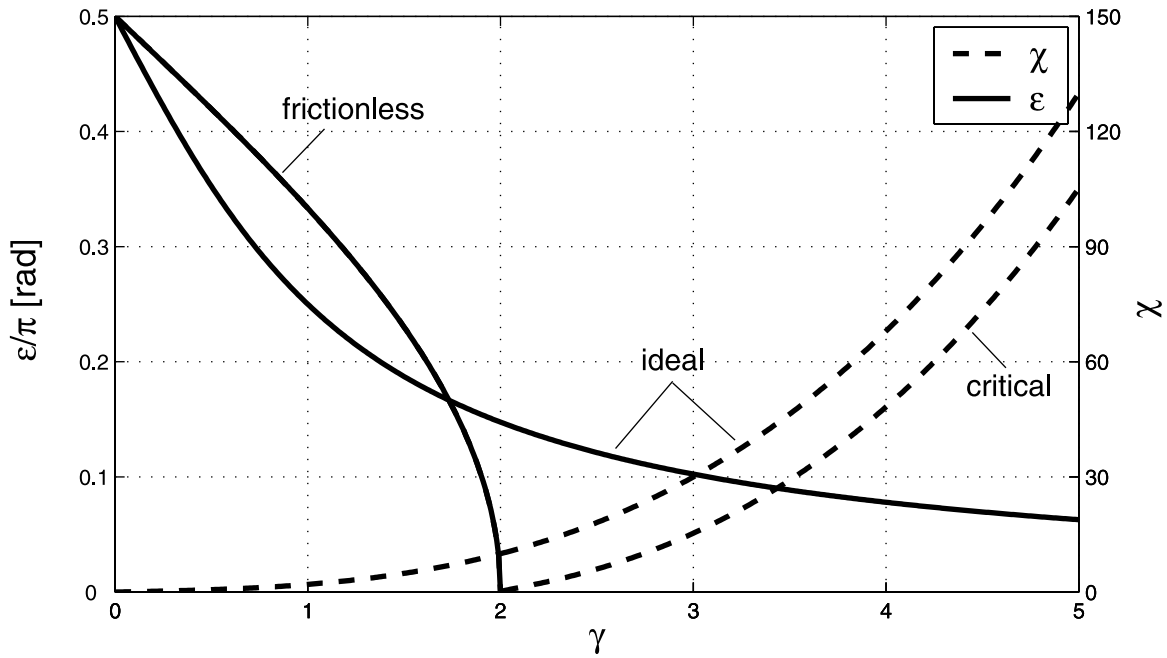$$\delta = \frac{\mu^2}{\mu^2 + 1} (\gamma - \chi \mu^2 \lambda^2), \qquad (30)$$

Figure 2. Phase lag ε and friction parameter χ as a function of convergence parameter γ under special conditions: threshold line for critical convergence $\gamma_c(\chi)$ from equation (43), discriminating between the two families of solution; conditions for an ideal estuary $\chi_I(\gamma)$ and $\varepsilon_I(\gamma)$ from equations (61) and (62); and phase lag behavior in a frictionless estuary from equation (68).

Celerity equation

$$\lambda^2 = 1 - D = 1 - \delta \frac{\cos \varepsilon}{\mu} = 1 - \delta(\gamma - \delta). \qquad (31)$$

[23] This is an implicit set of four equations that can compute: the celerity of tidal wave propagation, the tidal damping/amplification, the phase lag and the velocity amplitude for a given geometry, friction coefficient, and tidal amplitude to depth ratio. We see that the St. Venant's equations (1) and (2) are two equations with two unknowns (U and h) for given topography and friction, as a function of x. Equations (28)–(31) form a set of four equations with four unknowns (ε, λ, δ and μ) that can be solved for a given topography γ, and friction χ. It was recognized by *Jay* [1991], building on previous work by *Green* [1837] and *Prandle and Rahman* [1980], that the two main factors governing tidal propagation are friction and convergence. In this paper these factors are described by γ and χ, similar to parameters $-\Delta l$ and R'/ω of *Jay* [1991].

[24] The effect of the storage ratio r_S has already been included in the dimensional scaling. We also note that the friction parameter χ linearly depends on the dimensionless tidal amplitude ζ. It is, in fact, through the friction parameter that the tidal range to depth ratio comes into the equations. Hence, we consider γ and χ as the independent variables and ε, λ, δ, and μ as the dependent variables (see *Toffolon et al.* [2006] for an estuarine characterization in terms of external variables).

[25] Equations (28)–(31) represent a local solution, because they relate the velocity amplitude, the phase and

length of the tidal wave and the amplitude longitudinal variation (amplification or damping) to the local reference value of the tidal amplitude η itself (along with the geometrical characteristics of the channel).

3. Solution of the Set of Equations

[26] The set of equations (28)–(31) can be solved iteratively, but it is also amenable to an analytical solution, as shown by *Toffolon et al.* [2006]. Given the nonlinear character of the system, different families of solutions can be derived.

[27] Making use of the trigonometric equation $(\cos \varepsilon)^{-2} = 1 + (\tan \varepsilon)^2$, equations (28) and (29) can be combined to eliminate the variable ε to give

$$(\gamma - \delta)^2 = \frac{1}{\mu^2} - \lambda^2. \qquad (32)$$

Equations (30) and (31) can be rewritten as

$$\gamma - \delta = \chi \mu^2 \lambda^2 + \frac{\delta}{\mu^2}, \qquad (33)$$

$$\gamma - \delta = \frac{1 - \lambda^2}{\delta}. \qquad (34)$$

Isolating λ^2 from equation (34) and substituting into equations (32) and (33), we can write two equations in
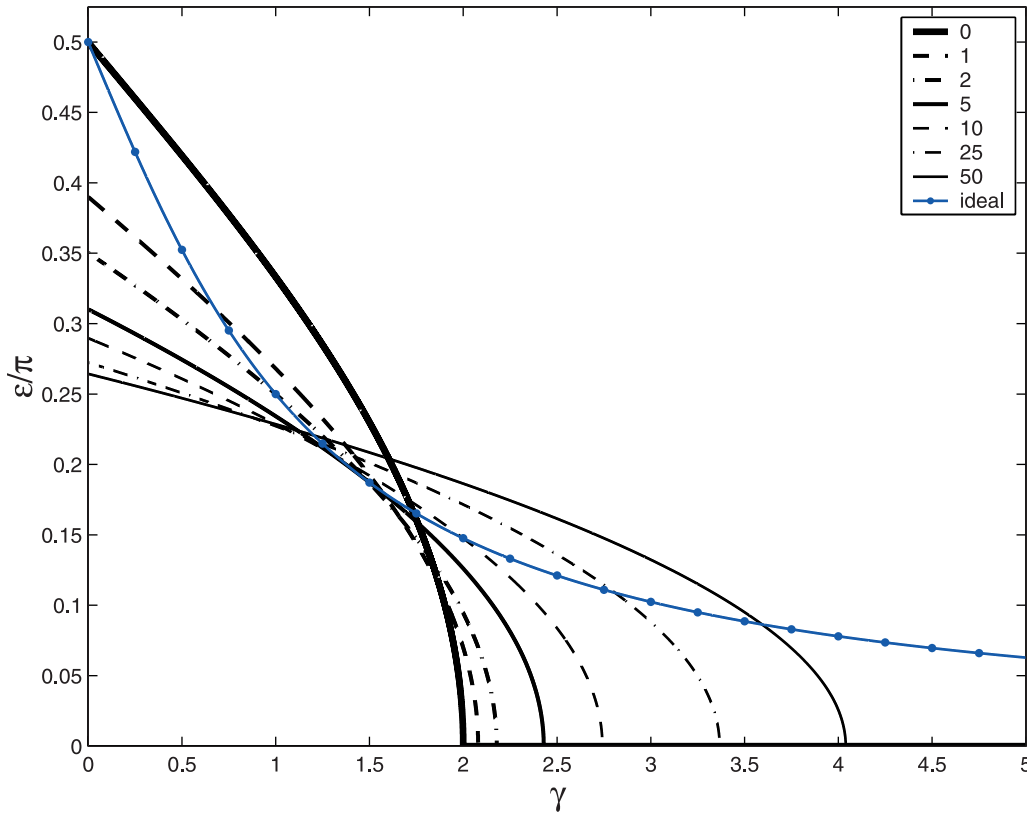
Figure 3a. Phase lag diagram showing the relationship between ε/π and the estuary shape number γ for different values of the friction number χ, indicated by different line types. The blue line with dots represents the ideal estuary (equation (63)).

the unknowns δ and μ. After some algebra, it is possible to obtain a single tenth-order equation for μ:

$$\frac{(\chi^2\mu^6 + \gamma\chi\mu^4 + 2\mu^2 - 2)(\mu^2 - \gamma\mu + 1)(\mu^2 + \gamma\mu + 1)}{\mu^2(\gamma\chi\mu^4 + 2\mu^2 + 2)} = 0. \tag{35}$$

The denominator of equation (35) is always strictly positive in the physically meaningful cases. Concerning the numerator, the relationships delimited by the first and second parentheses give rise to two different families of solutions (the first family representing the mixed tidal wave and the second family the "apparent standing" wave), which will be considered separately below. The equation delimited by the third parenthesis gives no positive roots for μ.

3.1. Solution for the Mixed Wave: First Family of Solutions

[28] We can now derive simpler relationships considering only a single family of solutions. Introducing equations (33) and (34) into equation (32), we end up with

$$\lambda^2\left[\delta\left(1 - \frac{1}{\mu^2}\right) + \chi\mu^2(1 - \lambda^2)\right] = 0, \tag{36}$$

which can be simplified for $\lambda^2 \neq 0$, neglecting the second family of solution. In this case, equation (36) along with equation (33) gives a simple relation between δ and μ:

$$\delta_m = \frac{\gamma - \chi\mu_m^2}{2}, \tag{37}$$

where the subscript m denotes the mixed tidal wave. Substituting equation (37) into equation (34), it is also possible to find

$$\lambda_m^2 = \frac{\chi^2\mu_m^4 - \gamma^2}{4} + 1. \tag{38}$$

These two equations for δ_m and λ_m can be used to eliminate δ and λ from equation (32). This leads to a single equation for μ_m:

$$\chi^2\mu_m^6 + \gamma\chi\mu_m^4 + 2\mu_m^2 - 2 = 0, \tag{39}$$

which corresponds to the first family of solution of equation (35) and represents the propagation of a mixed wave with $0 < \varepsilon < \pi/2$. It can be solved as a third-order equation in μ^2. The real solution is

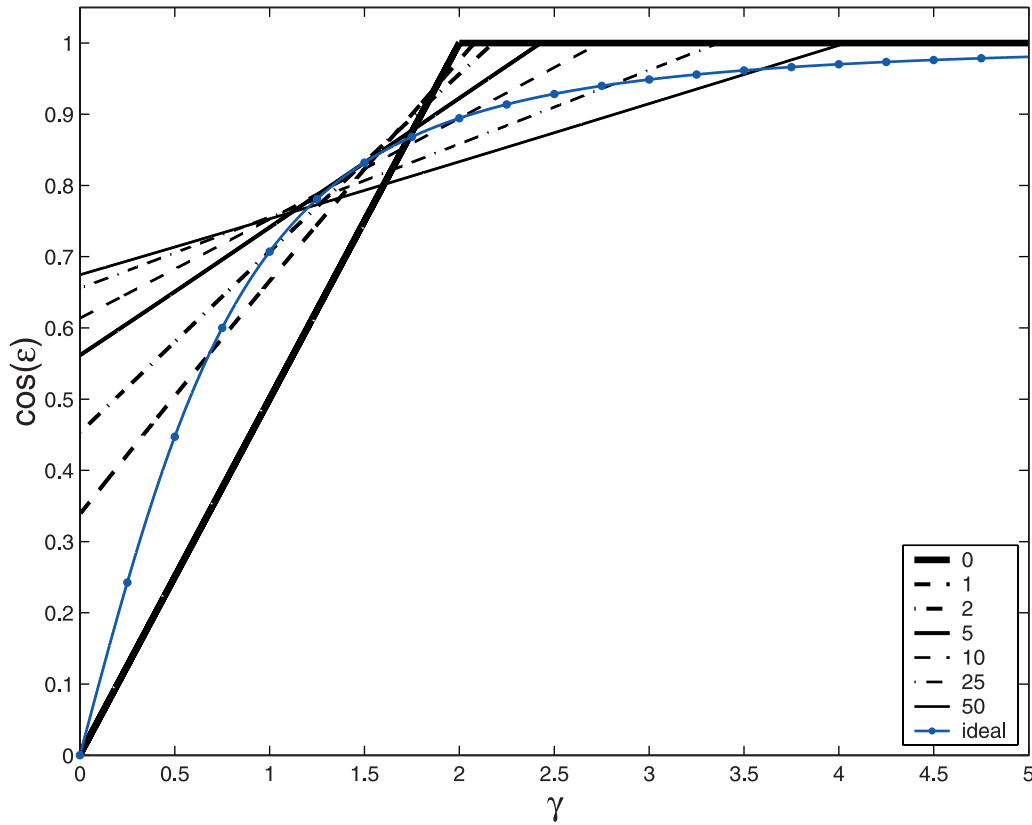$$\mu_m = \sqrt{\frac{1}{3\chi}\left(m - \gamma + \frac{\gamma^2 - 6}{m}\right)}, \tag{40a}$$

Figure 3b. Relationship between cos ε and the estuary shape number γ for different values of the friction number χ, indicated by different line types. The blue line with dots represents the ideal estuary (equation (64)).

$$m =$$
$$\left[27\chi + \left(9 - \gamma^2\right)\gamma + 3\sqrt{3}\sqrt{27\chi^2 + 2\left(9 - \gamma^2\right)\gamma\chi + 8 - \gamma^2} \right]^{1/3},$$
$$\tag{40b}$$

With this solution for μ_m, explicit solutions can be obtained for λ_m, δ_m, and ε_m, by substitution into equations (38), (37), and (28), respectively.

[29] Equations analogous to equation (39) can be written also for the other unknowns. For instance, the equation for λ reads

$$16\lambda_m^6 + 8\left(\gamma^2 - 4\right)\lambda_m^4 + \left[\left(\gamma^2 - 4\right)^2 + 4(\gamma\chi + 1)\right]\lambda_m^2$$
$$- \left[\chi^2 - \left(\gamma^2 - 4\right)(\gamma\chi + 1)\right] = 0, \tag{41}$$

which can be seen as a third-order equation in λ_m^2. The solution is physical only if real roots exist, that is, if $\lambda^2 \geq 0$. If $\lambda^2 = 0$, the threshold condition, according to equation (41), reads

$$\chi^2 - \left(\gamma_c^2 - 4\right)(\gamma_c\chi + 1) = 0, \tag{42}$$

where γ_c is the limit for critical convergence, defined as the threshold condition for the transition from the mixed tidal wave (first family of solutions) to the "apparent standing" wave (second family). Below we show that the second family of solution is completely determined by the convergence alone. Hence, critical convergence can also be defined as the limit for which the solution is influenced by friction. For weak friction, this boundary for critical convergence is similar to the one defined by *Jay* [1991] as the convergence rate at which convergence and acceleration effects are equal and opposed. For a frictionless tidal wave $\gamma_c = 2$, which is the same value as obtained by *Jay* [1991]. At this point the phase lag approaches zero, which is similar to the impedance phase ϕ of 90°, obtained by *Jay* [1991]. On the other hand, when friction becomes important, the two definitions of critical convergence lead to different results.

[30] The relationship in equation (42) defines the region of existence of critical convergence in the χ-γ plane and can be solved for one of the two parameters as a function of the other one. The expression for χ where $\gamma = \gamma_c$ reads

$$\chi(\gamma_c) = \frac{1}{2}\gamma_c\left(\gamma_c^2 - 4\right) + \frac{\left(\gamma_c^2 - 2\right)}{2}\sqrt{\gamma_c^2 - 4}, \tag{43}$$

where the condition $\gamma_c \geq \sqrt{2}$ (always satisfied, because $\gamma_c \geq 2$ as shown below) has been used to simplify the solution. The solution for γ is a more complex expression:

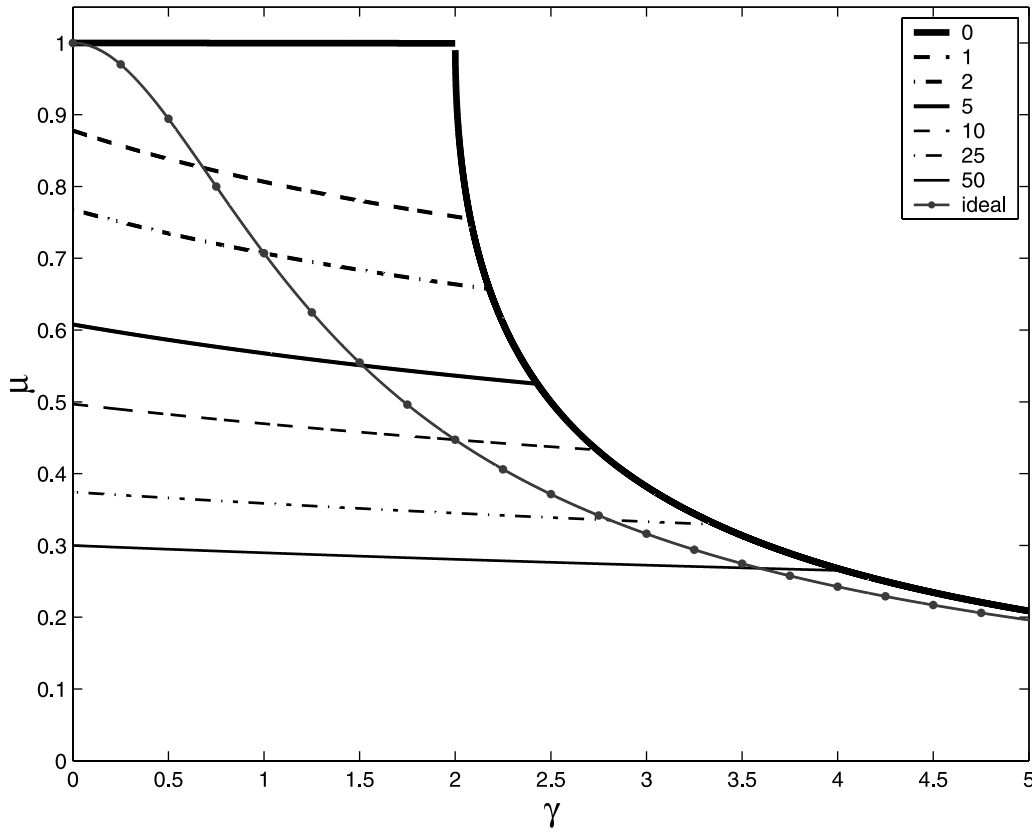$$\gamma_c = \frac{1}{3\chi}\left[\frac{m_1}{2} - 1 + 2\frac{\left(12\chi^2 + 1\right)}{m_1}\right], \tag{44a}$$

Figure 4. Relationship between the velocity number μ and the estuary shape number γ for different values of the friction number χ, indicated by different line types. The blue line with dots represents the ideal estuary (equation (60)).

$$m_1 = \left[36\chi^2(3\chi^2 + 8) - 8 + 12\chi\sqrt{3}\sqrt{(\chi^2 - 2)^2(27\chi^2 - 4)} \right]^{1/3}.$$

(44b)

The threshold condition is shown in Figure 2: the solution for the mixed wave exists for $\gamma < \gamma_c(\chi)$, where γ_c is the threshold for critical convergence, which increases with χ starting from $\gamma_c = 2$ for the frictionless case.

3.2. Solution for an Estuary With Constant Cross Section

[31] A special case of the mixed wave solution is the situation where there is no convergence, that is, when $\gamma = 0$. In that case, equations (37), (29), and (31) yield

$$\delta_0 = -\mu_0^2 \frac{\chi}{2},$$

(45)

$$\cos \varepsilon_0 = -\mu_0 \delta_0 = \frac{\chi}{2} \mu_0^3,$$

(46a)

$$\tan \varepsilon_0 = -\frac{\lambda_0}{\delta_0} = -\frac{\sqrt{1 + \delta_0^2}}{\delta_0}$$

(46b)

$$\lambda_0^2 = 1 + \left(\frac{\chi \mu_0^2}{2} \right)^2,$$

(47)

where the subscript 0 denotes the zero convergence situation. Using equation (40), and the condition that $\gamma = 0$, we can derive explicit expressions for μ_0, δ_0, ε_0 and λ_0:

$$\mu_0 = \sqrt{\frac{m_0^2 - 6}{3 m_0 \chi}},$$

(48)

$$\delta_0 = -\frac{m_0^2 - 6}{6 m_0},$$

(49)

$$\cos \varepsilon_0 = \frac{1}{2\sqrt{\chi}} \left(\frac{m_0^2 - 6}{3 m_0} \right)^{3/2},$$

(50a)

$$\tan \varepsilon_0 = \sqrt{1 + \left(\frac{6 m_0}{m_0^2 - 6} \right)^2},$$

(50b)

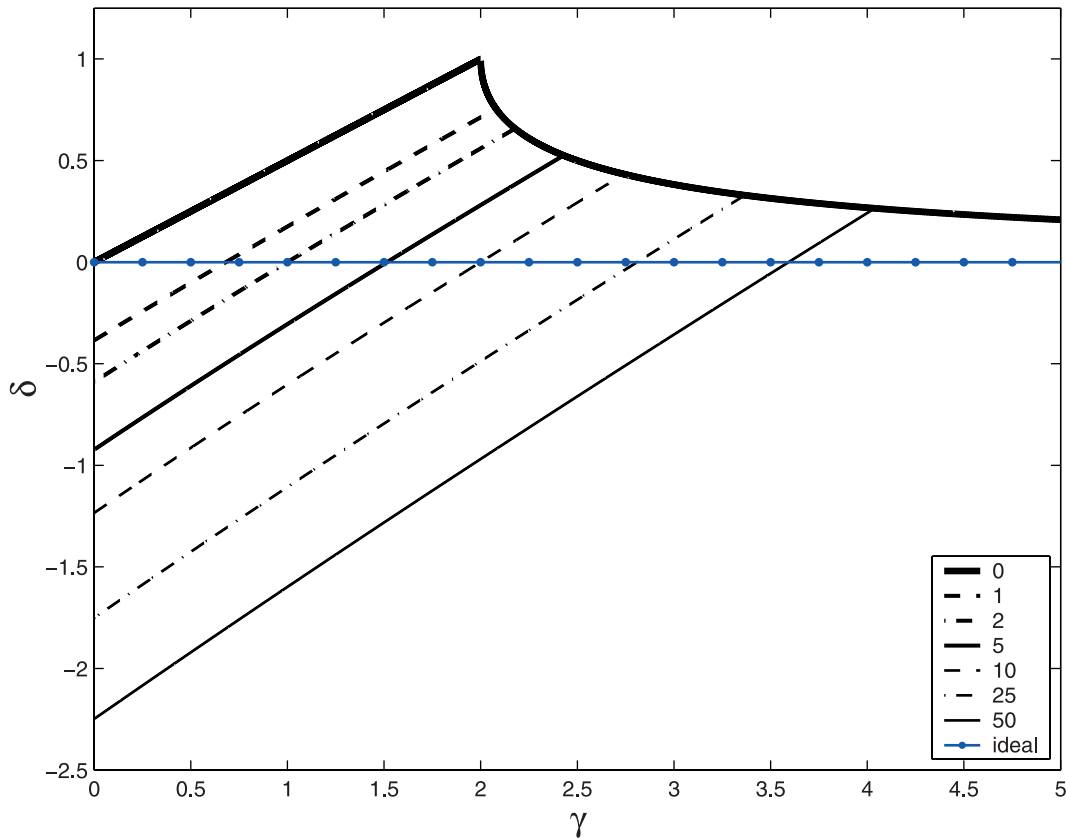$$\lambda_0^2 = 1 + \left(\frac{m_0^2 - 6}{6 m_0} \right)^2,$$

(51)

Figure 5. Relationship between the damping number δ and the estuary shape number γ for different values of the friction number χ, indicated by different line types. The blue line with dots represents the ideal estuary ($\delta = 0$).

$$m_0 = 3\left(\chi + \sqrt{\chi^2 + \frac{8}{27}}\right)^{1/3}. \tag{52}$$

[32] With these equations the damping and phase lag of a wave in an estuary with a constant cross section can be computed. We see that the damping, wave propagation and phase lag purely depend on the friction ratio, which is in agreement with the literature [e.g., *Lorentz*, 1926; *Lamb*, 1932; *Dronkers*, 1964; *Ippen*, 1966; *Van Rijn*, 1990]. In these solutions the tidal amplitude is damped exponentially and the tidal wave celerity is reduced accordingly. All these authors used linearized St. Venant equations and a constant damping number (exponential damping). As a result, their equations for the tidal wave propagation in a channel of constant cross section under the influence of friction are less accurate and less general than the solution presented here.

[33] In the special case of no friction we obtain $m_0 = \sqrt{6}$ and hence, as expected, that $\lambda_0 = 1$ (the classical wave celerity) and $\delta_0 = 0$ (no damping). One can also demonstrate that as χ approaches zero, μ_0 approaches unity and ε_0 approaches $\pi/2$: the case of the undamped progressive wave.

3.3. Solution for the Apparent Standing Wave: Second Family of Solutions

[34] It is also worthwhile to consider the solution in the case of an apparent standing wave (the wave is not a

standing wave in the formal sense; rather it is an incident wave that mimics a standing wave). For an apparent standing wave $\lambda = 0$ applies, which is the solution we have excluded in the simplification of equation (36) used to derive the first case. Imposing $\lambda = 0$ in the set of equations, we find that equation (32) is redundant since it is exactly the product of equations (33) and (34). Then, equating the latter two equations, one easily obtains

$$\mu_s^2 - \gamma\mu_s + 1 = 0, \tag{53}$$

$$\mu_s = \delta_s, \tag{54}$$

$$\varepsilon_s = 0, \tag{55}$$

where the subscript s stands for the standing wave solution, which pertains to the case where $\gamma > \gamma_c(\chi)$. The last equation follows directly from equation (28).

[35] This case corresponds to the second family of solutions of equation (35). Equation (53) gives real solutions only if $\gamma \geq 2$, which means beyond critical convergence; the physical solution hence reads

$$\mu_s = \frac{1}{2}\left(\gamma - \sqrt{\gamma^2 - 4}\right). \tag{56}$$

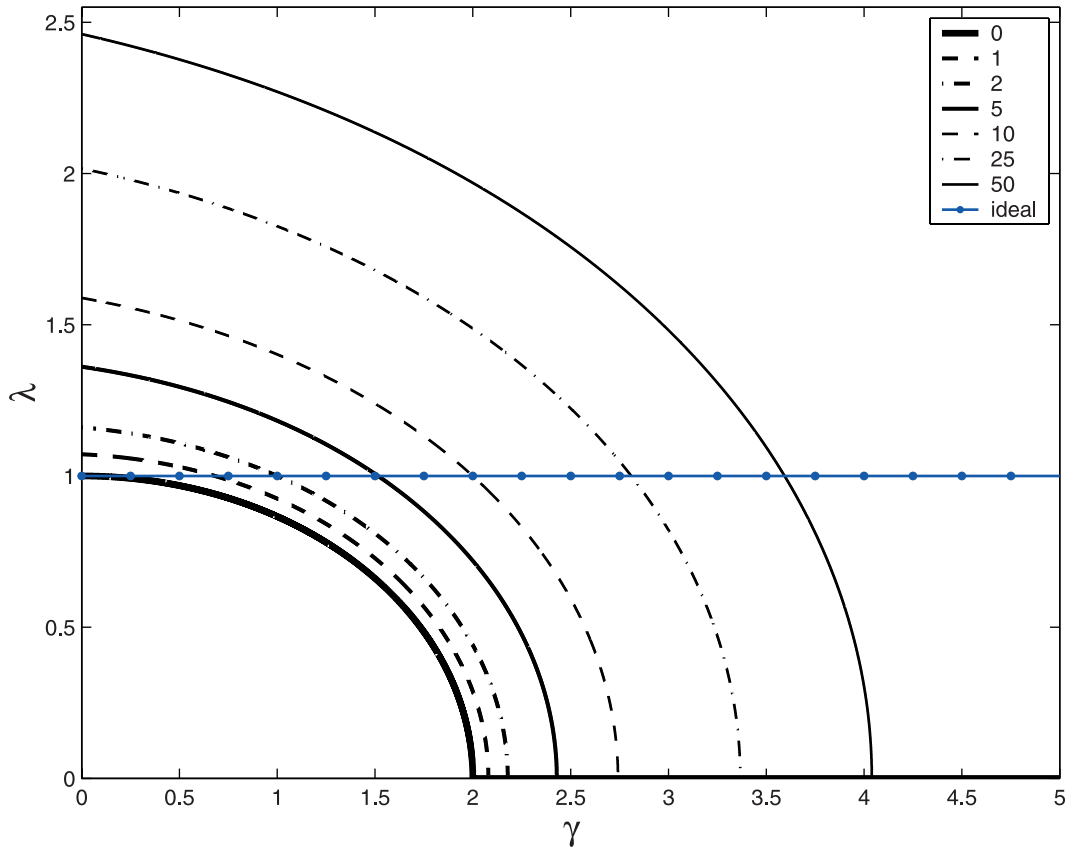If γ goes to infinity, this equation will approach $\mu_s = 1/\gamma$.

Figure 6. Relationship between the celerity number λ and the estuary shape number γ for different values of the friction number χ, indicated by different line types. The blue line with dots represents the ideal estuary ($\lambda = 1$).

[36] Similarly we can derive for the damping ratio,

$$\delta_s = \frac{1}{2}\left(\gamma - \sqrt{\gamma^2 - 4}\right), \tag{57}$$

which again gives the limit $\delta_s = 1/\gamma$ when γ goes to infinity.

[37] The threshold condition of equation (42) ensures that the transition between the two families of solution is smooth from the mixed tidal wave, given by equation (41), to the apparent standing wave where $\lambda = 0$. It is possible to demonstrate that also the transition between the solutions (40) and (56) is continuous.

3.4. Ideal Estuary

[38] An interesting special case of the first family of solutions (the mixed tidal wave) is that of the ideal estuary (subscript I), where there is neither tidal damping nor amplification. Hence, where

$$\delta_I = 0. \tag{58}$$

In this case, the system of equations (32)–(34) yields

$$\lambda_I^2 = 1, \tag{59}$$

$$\mu_I^2 = \frac{1}{\gamma^2 + 1} = \frac{\gamma}{\chi_I}, \tag{60}$$

which is the condition of solubility (representing the relationship between friction and convergence parameters necessary to obtain a balance between damping and amplification of the wave amplitude). This yields

$$\chi_I = \gamma(\gamma^2 + 1), \tag{61}$$

which has been tested against numerical results by *Toffolon et al.* [2006]. The phase lag can be estimated from equation (28):

$$\tan \varepsilon_I = \frac{1}{\gamma}. \tag{62}$$

[39] In addition, it follows from substitution of these values in equation (29) that

$$\sin \varepsilon_I = \sqrt{\frac{\gamma}{\chi_I}} = \sqrt{\frac{1}{\gamma^2 + 1}}, \tag{63}$$

$$\cos \varepsilon_I = \sqrt{\frac{\gamma^3}{\chi_I}} = \gamma\sqrt{\frac{1}{\gamma^2 + 1}}, \tag{64}$$

These relations for χ_I and ε_I are also presented in Figure 2.
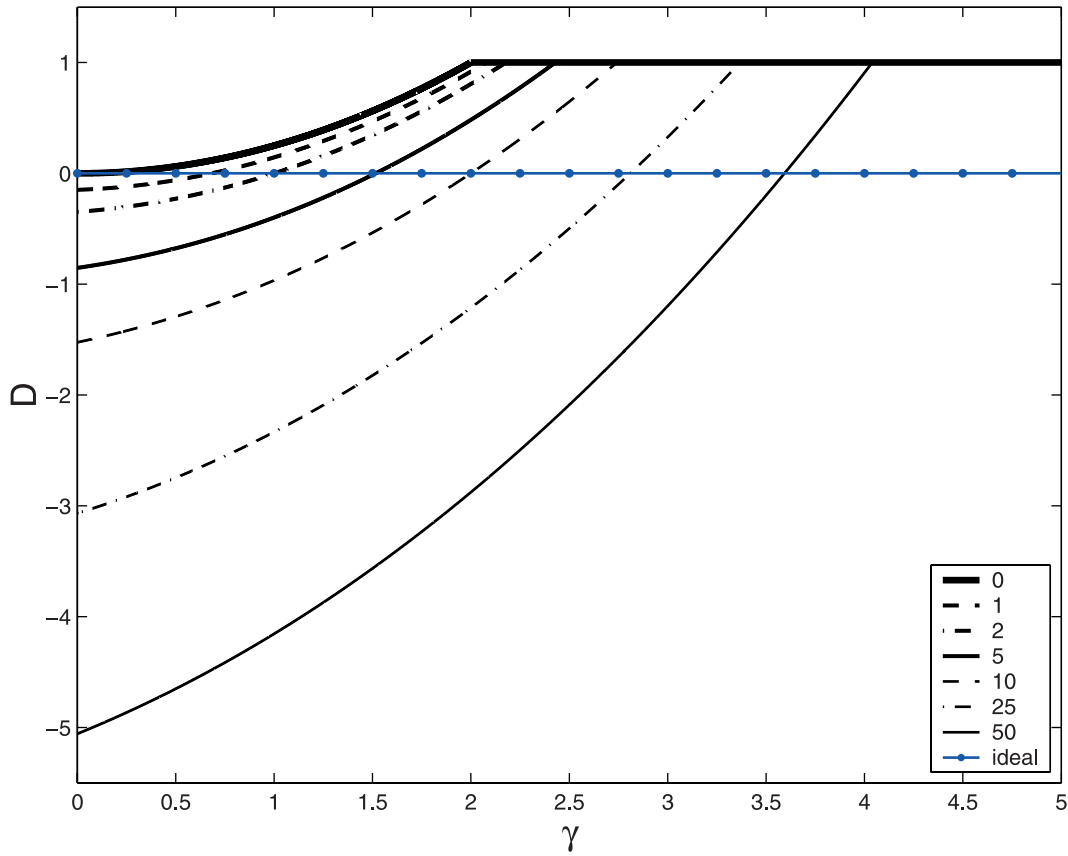
Figure 7. Relationship between the damping term D and the estuary shape number γ for different values of the friction number χ, indicated by different line types. The blue line with dots represents the ideal estuary ($D = 0$).

3.5. Frictionless Estuary

[40] Finally, a special case of the first family of solutions is the frictionless estuary. The second family of solutions, already is independent of friction. This is because in the damping equation (25) the friction is neutralized if $\varepsilon = 0$. In fact, an apparent standing wave has zero velocity at HW and LW and, as a result, the friction term falls out of the equation in the derivation of equation (25) [*Savenije*, 2001]. If a mixed wave has an infinitely small tidal amplitude, or if the estuary is frictionless, we also obtain $\chi = 0$. Under that condition, the expression for the velocity number (equation (39)) simplifies substantially, leading to

$$\mu_f = 1, \tag{65}$$

where the subscript f denotes the frictionless situation. In addition, we find

$$\delta_f = \gamma/2, \tag{66}$$

$$\lambda_f^2 = 1 - (\gamma/2)^2, \tag{67}$$

$$\cos \varepsilon_f = \gamma/2. \tag{68}$$

The resulting expression for ε_f is shown in Figure 2. The special case of a frictionless estuary with constant cross section ($\gamma = 0$) results in a purely progressive wave, with $\varepsilon = \pi/2$, $\delta = 0$ and $\lambda = 1$.

[41] In the next section, the curves representing the frictionless situation will be clearly visible in the graphical representations. The equations for δ_f and $\cos(\varepsilon_f)$ are simply straight lines; the equation for λ_f^2 is a parabola. Surprisingly, the equations describing $\cos(\varepsilon)$ and δ appear to behave as near-straight lines for the cases with friction as well.

4. Results and Discussion

4.1. Graphical Representation

[42] Figures 3–7 present the solution of the phase lag, the velocity number, the damping number, the celerity number and the damping number as a function of γ and χ. What we see very clearly in Figures 3–7 is that there exist two distinct types of estuaries that show very different behavior. For large values of γ (the strongly convergent estuaries) we see a behavior that no longer depends on the friction parameter χ and which corresponds to an apparent standing wave (the second family of solutions, where $\varepsilon = 0$). In this solution, $\lambda = 0$, implying an infinite celerity or, equivalently, an infinite wavelength; thus HW and LW occur instantaneously along the estuary. For smaller values of γ (the weakly convergent estuaries) we see a pattern that is strongly dependent on χ and which corresponds to the class
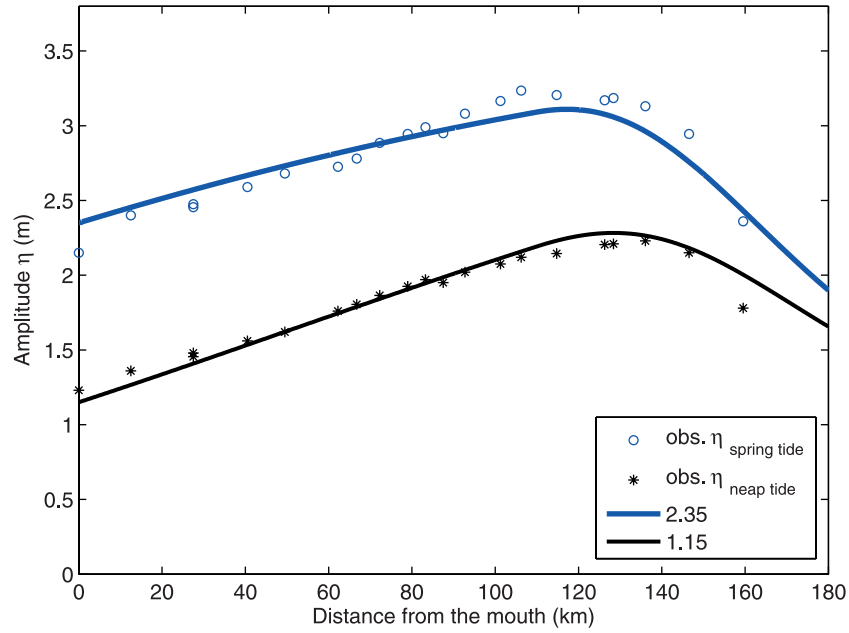
Figure 8a. Comparison between analytically evaluated tidal amplitude (continuous lines) and measurements (points) in the Schelde estuaries at different dates.

of estuaries with a mixed tidal wave (the first family of solutions, where $0 < \varepsilon < \pi/2$).

[43] The transition zone in the middle is the area where critical convergence occurs (with values of $\gamma > 2$). The set of points where critical convergence occurs is described by equation (42), with as a special point the frictionless critical convergence, where $\gamma_c = 2$. This frictionless critical convergence coincides with the corresponding critical convergence described by *Jay* [1991] and defines the point where the tidal wave approaches a standing wave owing to the convergence of the banks. Tidal waves are of the apparent standing wave type in short estuaries that are forced by a steep topography (as described, e.g., by *Wright et al.* [1973]); estuaries with a mixed tidal wave occur in river valley estuaries with a long coastal plain, as described by *Savenije* [2005]. In the former case the length of the estuary is typically one quarter of a wavelength (with a node at the upstream end of the estuary), whereas the latter is much longer. We see that for a very small tidal amplitude ($\chi \approx 0$), or frictionless wave, this happens at $\gamma = 2$, or at a
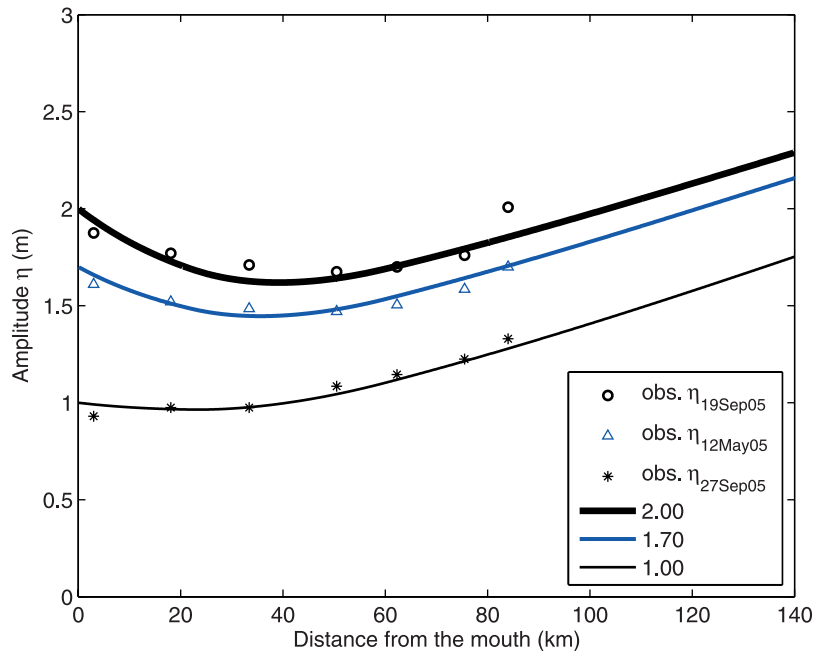

Figure 8b. Comparison between analytically evaluated tidal amplitude (continuous lines) and measurements (points) in the Elbe estuaries at different dates.

Table 2. Geometric and Tidal Characteristics of the Estuaries Studied

Estuary Name	Amplitude η_0 (m)	Reach (km)	Depth $\bar{h}$ (m)	Estuary Length L_e (km)	Cross-Sectional Area $\bar{A}_0$ (m^2)	Convergence Length a (km)	Storage Width Ratio r_S	River Discharge Q_f (m^3/s)
Elbe	1.5	0−60	7.0−9.0[a]	141	125,000	30[b]	1.7−1.2[c]	300
		60−140	9.0			30	1.2−1.0	
Schelde	1.9	0−110	10.5	192	260,000	28	1.7	40
		110−180	10.5−4.0			14	1.7−1.0	
Hau	1.4	0−57	5.5−10.0	300	26,600	105	1.2−1.0	950
		57−160	10.0			140	1.0	
Tien	1.2	0−45	6.4−7.7	300	21,600	71	1.2−1.0	700
		45−180	7.7			420	1.0	

[a]A value of 7.0−9.0 means a depth increase from 7.0 to 9.0 m over the reach 0−60 km.
[b]A value of 30 means a convergence length of 30 km over the reach 0−60 km.
[c]A value of 1.7−1.2 means a storage width ratio of 1.7−1.2 over the reach 0−60 km.

wavelength $L_0 = 4\pi a$. According to *Wright et al.* [1973], short estuaries with a standing wave have a length of $L_0/4$. Apparently the critical convergence for an estuary to develop an apparent standing wave (under near frictionless conditions) is $L_0/(4\pi)$, and the length of the estuary is πa. Substitution of this length in equation (6) shows that this corresponds to a point where the cross-sectional area has reduced to 4% of the area at the mouth: $\bar{A}/\bar{A}_0 = \exp(-\pi) \approx$ E0.04.

[44] In Figures 3a and 3b we see how the phase lag develops as a function of γ and χ. Figure 3a shows the phase lag diagram for estuaries with different convergence and friction. It also shows the phase lag of the ideal estuary.

Figure 3b shows the relationship between $\cos(\varepsilon)$, γ and χ. It is astonishing that the curves for $\cos(\varepsilon)$ appear as straight lines. The frictionless case is indeed a straight line, according to equation (68), but the curves for $\chi > 0$ only approach straight lines. The intercept of the line is given by equation (46), and the line reaches $\cos(\varepsilon) = 1$ at $\gamma = \gamma_c$, according to equation (44).

[45] In Figure 4 we see that the maximum value of the velocity number, $\mu = 1$, is reached for $\chi = 0$. The curves clearly have two branches, representing the two families of solutions. At critical convergence the curves change from a near linear relation to a hyperbole-like curve, earlier
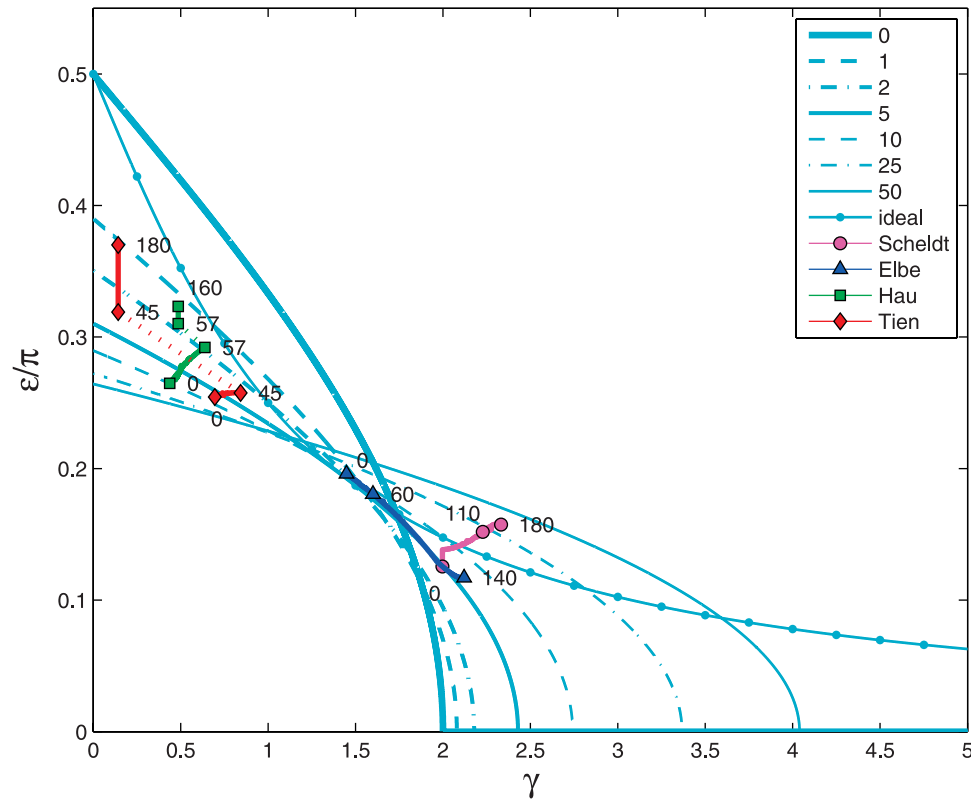

Figure 9. Positioning of the Schelde (purple circles), Elbe (blue triangles), Tien (red diamonds), and Hau (green squares) estuaries in the phase lag diagram, the numbers at inflection points indicating the distance from the estuary mouth (in kilometers). The background shows lines with different values of the friction number χ. The drawn line with the dots represents the "ideal" estuary.
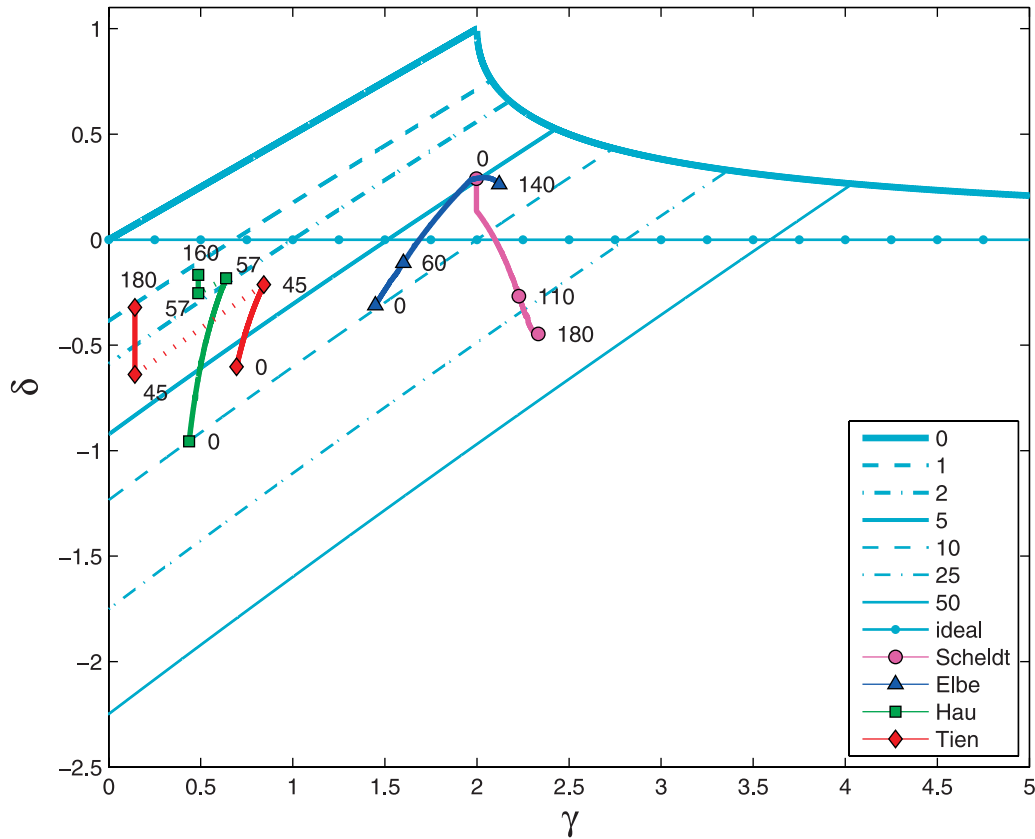
Figure 10. Positioning of the Schelde (purple circles), Elbe (blue triangles), Tien (red diamonds), and Hau (green squares) estuaries in the damping number diagram, the numbers at inflection points indicating the distance from the estuary mouth (in kilometers). The background shows lines with different values of the friction number χ. The drawn line with the dots represents the "ideal" estuary.

described by *Toffolon et al.* [2006]. The curve obeys equation (56) and for high values of γ tends to $\mu \approx 1/\gamma$.

[46] Figure 5 shows a similar picture for the damping number δ. For lower values of the estuary shape number, almost straight lines are found, which change into a hyperbole after the transition zone. In the frictionless case equation (66) applies as an exact straight line. The intercepts of these lines correspond to equation (49). The transition of the lines to the hyperbole occurs at critical convergence where $\gamma = \gamma_c$. Beyond critical convergence, equation (57) applies, which approaches $\delta = 1/\gamma$ for large values of γ. In this region there is always amplification, albeit modest. The line where $\delta = 0$ corresponds with the set of ideal estuaries. The point where both $\delta = 0$ and $\gamma = 0$ corresponds with the frictionless progressive wave.

[47] Figure 6 shows a similar picture for the celerity number λ. Ideal estuaries occur where $\lambda = 1$. Tidal damping corresponds with a wave celerity below the classical wave celerity ($\lambda > 1$); tidal amplification corresponds with a wave propagation that exceeds the classical wave celerity ($\lambda < 1$). Figure 7, which is closely related to Figure 6, shows that the damping term $D = 1$ for large values of γ.

[48] What we cannot see from Figures 6 and 7 is how in a given estuary, with a given topography and friction, the parameters change as a function of x, because ζ, and hence χ, is not necessarily constant with x. Only in an ideal estuary, where ζ is constant and hence all parameters are

fixed for a given value of γ, estuaries can be characterized by a single dot in these graphs. If these variables are not constant, then an estuary is represented by a line segment. For a constant value of γ this is a vertical line segment. If γ varies along the estuary axis (e.g., because of shallowing), then the line segments can go across the graphs. In the following section the methodology to draw such a line segment is presented and subsequently examples of real estuaries are given.

4.2. Longitudinal Solution for Tidal Wave Propagation in Real Estuaries

[49] To represent the estuary parameters of tidal wave propagation along the estuary axis, a longitudinal solution is required. The water level variation along the estuary axis cannot be read directly from the derived equations, but it is described by the integration of the damping number δ.

[50] The computation depends on the two independent variables γ and χ. For a given topography, storage width ratio and friction factor, the value of γ can be computed, but χ still depends on the tidal amplitude, which can only be obtained from integration of the damping number. This is done by simple explicit integration of the linear differential equation. Hence, the set of equations can be solved by selecting a tidal amplitude at the seaward boundary η_0, and by integration of the damping number over a distance Δx,
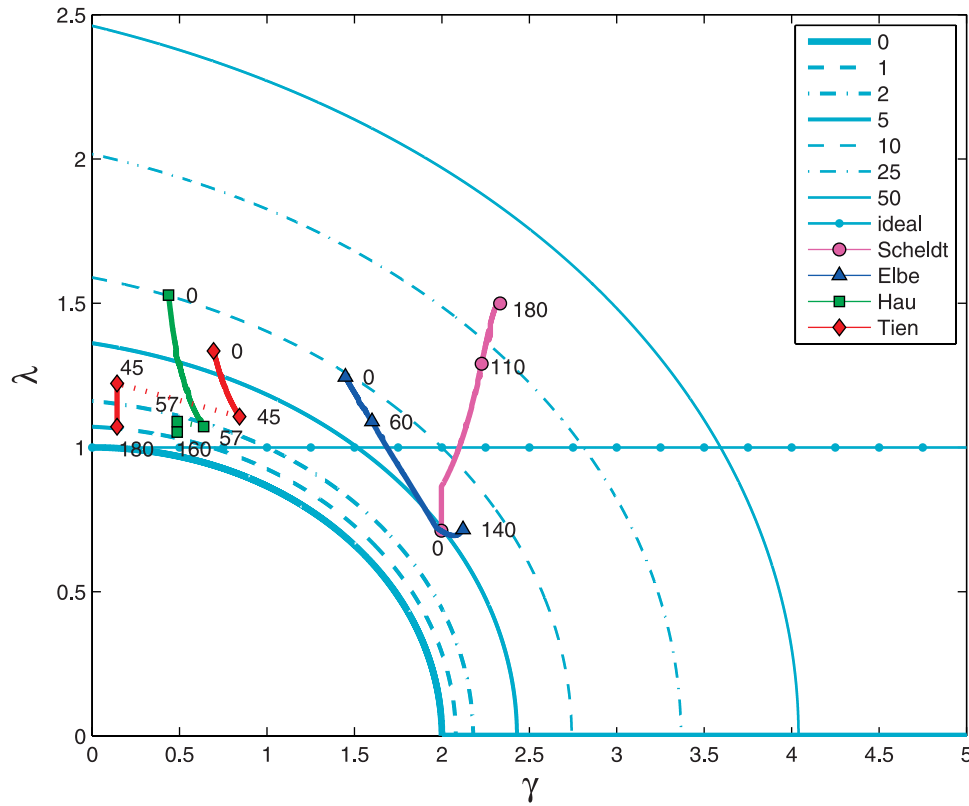
Figure 11. Positioning of the Schelde (purple circles), Elbe (blue triangles), Tien (red diamonds), and Hau (green squares) estuaries in the celerity number diagram, the numbers at inflection points indicating the distance from the estuary mouth (in kilometers). The background shows lines with different values of the friction number χ. The drawn line with the dots represents the "ideal" estuary.

leading to a tidal amplitude η_1 at a distance Δx upstream, which is repeated for the entire length of the estuary.

[51] Figures 8a and 8b show the longitudinal computation applied to the Schelde (Figure 8a) and Elbe (Figure 8b) estuaries at different dates, with different tidal amplitudes. In both estuaries, the correspondence with observations is good. Table 2 presents data of the Schelde, Elbe, Tien (Mekong), and Hau (Mekong) on which these computation and the ones in the next section are based. Chezy's coefficient has been determined with the Strickler-Manning relation $C = K\overline{h}^{1/6}$ with $K = 45 \ \mathrm{m}^{1/3} \ \mathrm{s}^{-1}$.

4.3. Comparing Different Estuaries

[52] In Figures 9–12 we see the graphs for the phase lag, the celerity number, the damping number and the velocity number. In these graphs the Schelde, Elbe, Tien, and Hau estuaries are represented by line segments of red, blue, dark green, and light green color, respectively. Next to the segments the distance in km is written indicating the length over which a segment is representative. We can see that in the Schelde the downstream parts of 0–110 km forms a vertical line segment with a constant estuary shape number. Further upstream the pattern becomes more irregular owing to shallowing. The Hau has a constant reach from 57 to 160 km and the Tien from 45 to 180 km. The Elbe has a less regular depth profile and hence does not have a constant estuary shape number. For the data used, reference is made to Table 2. The tidal amplitude represents a normal spring tide and the river discharge an indication of dry season flow.

[53] Of the four estuaries, the Tien and the Hau have the smallest estuary shape number. They are clearly under the influence of river discharge, which causes these estuaries to experience more damping than an ideal estuary would. They have a riverine character with a long convergence length and a high phase lag. The Schelde is a more marine estuary with the largest estuary shape number, the smallest phase lag (closest to the apparent standing wave) and it is amplified. The Elbe lies in between; the tidal wave is not much damped nor amplified and the estuary behaves almost as an ideal estuary.

[54] In Figure 9 we see that there is a transition range near $\gamma = 1.5$ where the lines for different values of χ cross. For lower estuary shape numbers, the phase lag decreases with friction; for higher values, the phase lag increases with friction. In the transition zone, the range of phase lags is very small and not very sensitive to friction (around 70 min for an M_2 tide). The Elbe lies in this transition zone. We see that the natural estuaries lie close to the line of the ideal estuaries. Marine estuaries experience amplification if they lie below the line of the ideal estuary; riverine estuaries, however, experience damping if they lie below the line.

5. Conclusions

[55] The explicit analytical solutions and the graphs presented in this paper offer the opportunity to look into the functioning of the St. Venant equations, without the need for a hydrodynamic model. In fact they allow us to
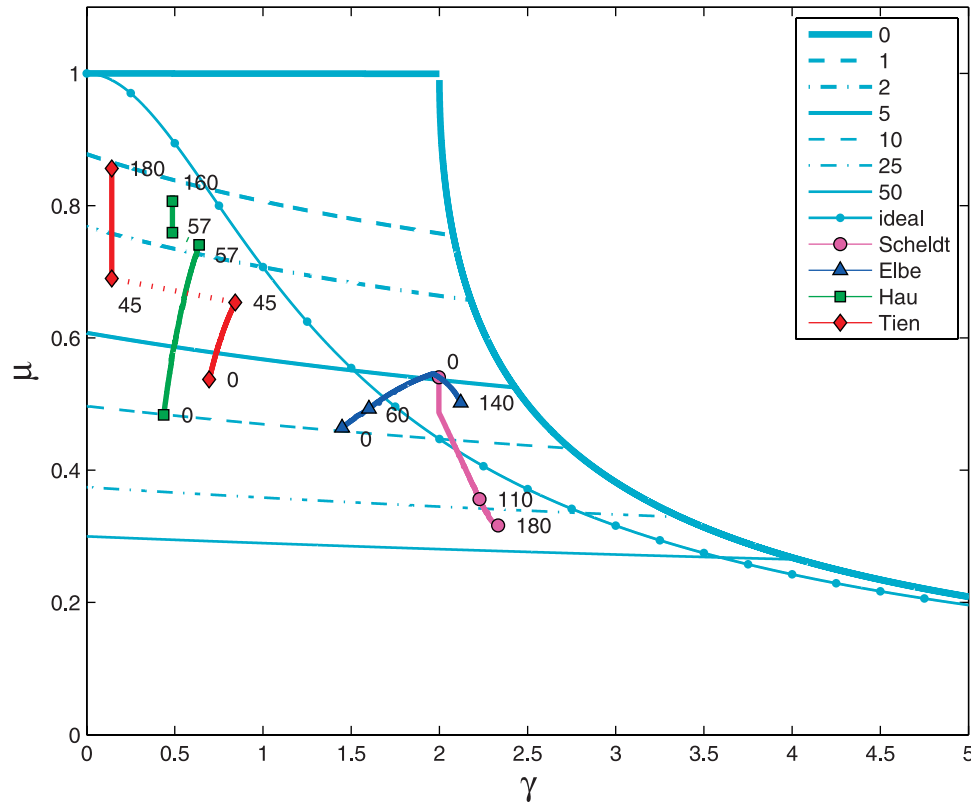
Figure 12. Positioning of the Schelde (purple circles), Elbe (blue triangles), Tien (red diamonds), and Hau (green squares) estuaries in velocity number diagram, the numbers at inflection points indicating the distance from the estuary mouth (in kilometers). The background shows lines with different values of the friction number χ. The drawn line with the dots represents the "ideal" estuary.

determine the tidal velocity amplitude, the rate of tidal damping and the wave celerity directly on the basis of a geometry indicator, friction and tidal forcing. The method is accurate compared to earlier analytical methods and even very accurate in the marine part of an estuary where the tide dominates over the river discharge. This happens to be the area where salinity intrusion and estuary ecology is relevant, which makes this method very powerful to be combined with salt intrusion models, ecological models or decision support systems.

[56] In addition, the method can be used directly for the variable of interest, for example, the tidal amplitude, the velocity amplitude, the wave celerity, or the phase lag, without the need to look at the entire process. One only requires the local geometry, the tidal amplitude and the friction. Especially the phase lag between HW and HWS is not a parameter easily determined in other methods.

[57] The method shows a satisfactory comparison with field data, particularly in view of the simplicity of the geometric schematization. This indicates that the exponential function used is a natural shape of alluvial estuaries and that the function obeys natural laws of self-organization, in line with the "ideal estuary" [*Savenije*, 2005].

[58] This paper shows that classification of estuaries should be based on two parameters, the estuary shape number γ and the friction scale χ [see also *Toffolon et al.*, 2006]. The phase lag is a key parameter to classify an estuary. Since natural estuaries appear to follow the trend of

ideal estuaries, the position that an estuary has in Figure 9, identifies it as, for example, a riverine estuary with a low estuary shape number and a high phase lag which is mainly damped (Mekong), a marine estuary with a high estuary shape number and a small phase lag which is mainly amplified (Schelde), or a transitional estuary with an estuary shape number in the order of 1.5, a phase lag close to 0.2π (70 min for an M$_2$ tide) and almost zero damping (Elbe).

Notation

a	convergence length of cross-sectional area, L.
A	cross-sectional area of flow, L^2.
A_0	cross-sectional area at the mouth, L^2.
c	wave celerity, LT^{-1}.
c_0	classical wave celerity, LT^{-1}.
C	Chezy's friction factor, L$^{1/2}$ T^{-1}.
D	damping term.
E	tidal excursion, L.
f	friction factor.
g	acceleration due to gravity, LT^{-2}.
h	cross-sectional average depth of flow, L.
K	Manning-Strickler friction factor, L$^{1/3}$ T^{-1}.
L	wavelength, L.
L_0	classical wavelength, L.
L_e	estuary length, L.
m	parameter.
Q	tidal discharge, L^3 T^{-1}.

Q_f freshwater discharge, $L^3 T^{-1}$.

r_S storage width ratio.

t time, T.

T tidal period, T.

U cross-sectional average flow velocity, LT^{-1}.

x distance, L.

z water level, L.

z_b bottom level, L.

γ estuary shape number.

δ damping number.

ε phase lag.

ζ tidal amplitude to depth ratio.

η tidal amplitude, L.

η_0 tidal amplitude at the mouth, L.

λ celerity number.

μ velocity number.

ρ density of water, ML^{-3}.

σ residual water level slope.

ϕ phase.

υ tidal velocity amplitude.

χ friction number.

ω tidal frequency, T^{-1}.

References

Dronkers, J. J. (1964), *Tidal Computations in Rivers and Coastal Waters*, Elsevier, New York.

Friedrichs, C. T., and D. G. Aubrey (1994), Tidal propagation in strongly convergent channels, *J. Geophys. Res.*, *99*(C2), 3321–3336.

Green, G. (1837), On the motion of waves in a variable canal of small depth and width, *Trans. Cambridge Philos. Soc.*, *6*, 457–462.

Harleman, D. R. F. (1966), Tidal dynamics in estuaries, part II: Real estuaries, in *Estuary and Coastline Hydrodynamics*, edited by A. T. Ippen et al., McGraw-Hill, New York.

Horrevoets, A. C., H. H. G. Savenije, J. N. Schuurman, and S. Graas (2004), The influence of river discharge on tidal damping in alluvial estuaries, *J. Hydrol.*, *294*(4), 213–228, doi:10.1016/j.jhydrol.2004.02.012.

Ippen, A. T. (1966), Tidal dynamics in estuaries, part I: Estuaries of rectangular section, in *Estuary and Coastline Hydrodynamics*, edited by A. T. Ippen et al., McGraw-Hill, New York.

Jay, D. A. (1991), Green's Law revisited: Tidal long-wave propagation in channels with strong topography, *J. Geophys. Res.*, *96*(C11), 20,585–20,598.

Lamb, H. (1932), *Hydrodynamics*, Cambridge Univ. Press, New York.

Lanzoni, S., and G. Seminara (1998), On tide propagation in convergent estuaries, *J. Geophys. Res.*, *103*, 30,793–30,812.

Lorentz, H. A. (1926), *Verslag Staatscommissie Zuiderzee* (in Dutch), Algemene Landsdrukkerij, The Hague, Netherlands.

Prandle, D. (2003), Relationships between tidal dynamics and bathymetry in strongly convergent estuaries, *J. Phys. Oceanogr.*, *33*, 2738–2750, doi:10.1175/1520-0485(2003)033<2738:RBTDAB>2.0.CO;2.

Prandle, D., and M. Rahman (1980), Tidal response in estuaries, *J. Phys. Oceanogr.*, *10*, 1552–1573, doi:10.1175/1520-0485(1980)010 <1552: TRIE>2.0.CO;2.

Savenije, H. H. G. (1992), Lagrangian solution of St. Venant's equations for an alluvial estuary, *J. Hydraul. Eng.*, *118*(8), 1153–1163, doi:10.1061/(ASCE)0733-9429(1992)118:8(1153).

Savenije, H. H. G. (1993), Determination of estuary parameters on the basis of Lagrangian analysis, *J. Hydraul. Eng.*, *119*(5), 628–643.

Savenije, H. H. G. (1998), Analytical expression for tidal damping in alluvial estuaries, *J. Hydraul. Eng.*, *124*(6), 615–618, doi:10.1061/(ASCE)0733-9429(1998)124:6(615).

Savenije, H. H. G. (2001), A simple analytical expression to describe tidal damping or amplification, *J. Hydrol.*, *243*, 205–215, doi:10.1016/S0022-1694(00)00414-5.

Savenije, H. H. G. (2005), *Salinity and Tides in Alluvial Estuaries*, Elsevier, New York.

Savenije, H. H. G., and E. J. M. Veling (2005), The relation between tidal damping and wave celerity in estuaries, *J. Geophys. Res.*, *110*, C04007, doi:10.1029/2004JC002278.

Toffolon, M., G. Vignoli, and M. Tubino (2006), Relevant parameters and finite amplitude effects in estuarine hydrodynamics, *J. Geophys. Res.*, *111*, C10014, doi:10.1029/2005JC003104.

Van Rijn, L. (1990), *Principles of Fluid Flow and Surface Waves in Rivers, Estuaries, Seas and Oceans*, Aqua, Amsterdam.

Wright, L. D., J. M. Coleman, and B. G. Thom (1973), Processes of channel development in a high tide range environment: Cambridge Gulf-Ord river delta, Western Australia, *J. Geol.*, *81*, 15–41.

———————

J. Haas, H. H. G. Savenije, and E. J. M. Veling, Department of Water Management, Delft University of Technology, P.O. Box 5048, NL-2600-GA Delft, Netherlands. (h.h.g.savenije@tudelft.nl)

M. Toffolon, Department of Civil and Environmental Engineering, University of Trento, Via Mesiano, 77, I-38100 Trento, Italy.